# Geophysical Research Letters®

# Ice Shelf Basal Melt Rates in the Amundsen Sea at the End of the 21st Century

Nicolas C. Jourdain[1] , Pierre Mathiot[1] , Clara Burgard[1] , Justine Caillet[1] , and Christoph Kittel[1]

[1]Institut des Géosciences et de l'Environnement, University Grenoble Alpes/CNRS/IRD/G-INP, Grenoble, France

**Abstract** Antarctic Ice Sheet projections show the highest sensitivity to increased basal melting in the Amundsen Sea. However, little is known about the processes that control future increase in melt rates. We build an ensemble of three ocean–sea-ice–ice-shelf simulations for both the recent decades and the late 21st century, constrained by regional atmosphere simulations and the multi-model mean climate change of the fifth Climate Model Intercomparison Project under the RCP8.5 scenario. The ice-shelf melt rates are typically multiplied by 1.4–2.2 from present day to future, for a total basal mass loss increased by 346 Gt yr$^{-1}$ on average. This is equally explained by advection of warmer water from remote locations and regional changes in Ekman downwelling and in the ice-shelf melt-induced circulation, while increased iceberg melt plays no significant role. Our simulations suggest that high-end melt projections previously used to constrain recent sea level projections may have been significantly overestimated.

**Plain Language Summary** Future sea level rise highly depends on how fast the ocean will melt the floating ice shelves in Antarctica, which modulates the ice flow from the ice sheet into the ocean. This is particularly true for the Amundsen Sea sector where the ice flow into the ocean is very sensitive to ocean-induced melting. Here, we use a numerical model that represents the evolution of the Amundsen Sea, including under the floating ice shelves. Under a high-end greenhouse-gases concentration pathway, our simulations indicate that melt rates beneath the ice shelves may increase by 40%–120%. This is explained by both warmer seawater coming from distant regions and changes in the local wind stress. Our simulations suggest that high-end melt projections previously used to constrain recent sea level projections may have been overestimated.

## 1. Introduction

Most projections of the Antarctic contribution to sea level rise are based on standalone ice sheet models in which melting beneath ice shelves is parameterized (DeConto et al., 2021; Edwards et al., 2021; Levermann et al., 2020; Seroussi et al., 2020). The existing melt parameterizations are based on highly simplified representations of the ocean circulation and heat exchanges in ice shelf cavities, and the resulting melt rates are significantly biased (Burgard et al., 2022; Favier et al., 2019). Furthermore, these melt parameterizations are typically driven by ocean warming derived from simulations of the Climate Model Intercomparison Project (CMIP, Eyring et al., 2016), although ice shelf cavities are not represented and ocean properties on the Antarctic continental shelf are significantly biased (Purich & England, 2021).

To either trust or challenge these ice sheet and sea level projections, our community needs projections that resolve the ocean dynamics over the Antarctic continental shelf and beneath the ice shelves, but such projections are rare (Asay-Davis et al., 2017). Timmermann and Hellmer (2013) and Naughten, Meissner, Galton-Fenzi, England, Timmermann, and Hellmer (2018) pioneered CMIP-based projections at the Antarctic scale, using a global ocean model with refined resolution around Antarctica and beneath ice shelves. Their projections were nonetheless of limited use for the Amundsen Sea sector because of a substantial cold bias in their present-day state. Siahaan et al. (2021) were the first to run a global climate model (i.e., land, ocean, atmosphere) with an interactive Antarctic Ice Sheet in scenario-based projections. Their present-day melt rates were reasonable in the Amundsen Sea, but they found little change in their projections and questioned the representation of the Amundsen cavities at their resolution (e.g., only 11 grid columns for Pine Island ice shelf cavity). Stronger present-day biases were nonetheless found at higher ocean resolution in their model configuration (Smith et al., 2021).

Given that the Antarctic Ice Sheet projections show the highest sensitivity to increased basal melting in the Amundsen Sea sector (together with the Wilkes Land sector, Seroussi et al., 2020), it seems crucial to better estimate possible future ice shelf melt rates in that region and describe the associated mechanisms. Recent simulations of the Amundsen Sea by Naughten et al. (2022) have shown that relatively warm periods become more dominant over the twentieth century, causing stronger ice shelf melting. In this paper, we use a regional ocean–sea-ice–ice-shelf model to build new projections to 2100 under the RCP8.5 scenario for the Amundsen Sea region and to describe the mechanisms explaining changes in ice shelf melt rates. High-end sea level projections are needed from an adaptation perspective (Durand et al., 2022; Hinkel et al., 2019), but are currently extremely uncertain, partly due to the poorly constrained sensitivity of ice shelf melt rates to ocean warming (Edwards et al., 2021; Fox-Kemper et al., 2021). This is our motivation to focus on the RCP8.5 scenario, which is on the higher end of possible scenarios in a world with no climate policy (Hausfather & Peters, 2020a, 2020b). Finally, we use our ocean projections to assess existing melt parameterizations recently used in ice sheet projections.

## 2. Ocean–Sea-Ice–Ice-Shelf Simulations

We make use of the NEMO-3.6 (Nucleus for European Modeling of the Ocean, Madec & NEMO-team, 2016) ocean model that includes the LIM3 (Louvain Ice Model, Rousset et al., 2015) sea ice model and the ice shelf cavity module developed by Mathiot et al. (2017). The grid extends from 142.1°W to 84.9°W and from 76.5°S to 59.7°S, and has a resolution of 1/12° in longitude, that is, a quasi-isotropic resolution varying from 4.7 km at the northern boundary to 2.2 km in the southernmost part of the domain. We use 75 vertical levels of thickness ranging from 1 m at the surface to 204 m at 6,000 m depth, and a typical thickness of 30–100 m for ocean cells beneath ice shelves. Unless stated otherwise, the parameters are those used in Jourdain et al. (2017) and the complete set of NEMO parameters is provided on https://doi.org/10.5281/zenodo.6644859.

To get a rough estimate of the model uncertainty, we run an ensemble of three present-day and future simulations. For ensemble member A, the ice shelf and seabed topography is extracted from BedMachine-Antarctica-v1.33 (Morlighem et al., 2020), while members B and C are based on BedMachine-Antarctica-v2.0 (Morlighem, 2020). Additionally, B and C include a representation of grounded tabular icebergs, in particular B22A (Antarctic Iceberg Tracking Database, Budge & Long, 2018), whose ungrounded parts are treated as an ice shelf, and the line of icebergs grounded on Bear Ridge (Bett et al., 2020; Nakayama et al., 2014). The ocean–ice-shelf heat exchange coefficient ($\Gamma_T$) is $2.21 \times 10^{-2}$ in A versus $1.88 \times 10^{-2}$ in B–C, while the ocean–ice-shelf salt exchange coefficient is always defined as $\Gamma_S = \Gamma_T/35$. Finally, two parameters of the sea ice model differ: the maximum permitted sea ice concentration is set to 99.9% of the mesh in A–B versus 95% in C, and the ice–ocean drag coefficient is set to $5.0 \times 10^{-3}$ in A–B versus $2.5 \times 10^{-3}$ in C. All these parameter values are commonly used in the NEMO community. Our ensemble is designed to simply illustrate the importance of a few empirical choices and cannot be considered as a deep exploration of NEMO's parametric uncertainty (e.g., Williamson et al., 2017).

Our present-day simulations cover 1989–2009, following 10 years of spin up from 1979. The surface boundary conditions consist of 3-hourly (temperature, humidity, wind velocity) and daily (radiative fluxes and precipitation) mean outputs of the 10 km MAR (Regional Atmospheric Model, Gallée & Schayes, 1994) configuration described and evaluated by Donat-Magnin et al. (2020). The lateral ocean and sea ice boundary conditions consist of 5-day mean outputs of a global 0.25° NEMO simulation very similar to the one described by Merino et al. (2018) except that it is spun up from 1958 and that the imposed ice shelf melt flux increases linearly from 1990 to 2005 and is constant before and after that, with values corresponding to the FRESH − and FRESH + reconstructions of Merino et al. (2018). The global 0.25° simulation represents Lagrangian icebergs (Merino et al., 2016), and their 5-day averaged melt rate (Jourdain, Merino, et al., 2019) is applied at the surface of our regional 1/12° configuration. In addition, seven tidal constituents are applied at the lateral boundaries as in (Jourdain, Molines, et al., 2019). Our present-day simulations are evaluated in Section S1 in Supporting Information S1. In summary, our simulations are too warm at depth by approximately 0.5°C, and ice shelf melt rates are consequently slightly overestimated.

Our future simulations cover 2080–2100 and are representative of the CMIP5 multi-model mean under the RCP8.5 concentration pathway. The surface boundary conditions are taken from the MAR regional projections described and evaluated through a perfect-model approach in Donat-Magnin et al. (2021). The atmospheric projections themselves were driven at their surface and lateral boundaries by the mean seasonal anomalies (2080–2100 minus 1989–2009) derived from 33 CMIP5 models under the RCP8.5 scenario (more details are provided in

Donat-Magnin et al., 2021). Our future simulations start from the 1979 ocean conditions (same as present-day) and are spun up for 10 years under future surface and lateral boundary conditions using the same method as for 2080–2100. Due to its open lateral boundaries, our regional ocean model configuration is no longer sensitive to its initial state after approximately 7 years (Jourdain et al., 2017), which means that starting our future runs from the present-day conditions is acceptable as long as we allow some years for spin up, and it is not required to simulate the entire 2010–2070 period to estimate melt rates at the end of the 21st century.

The applied anomalies induce an eastward zonal wind and sea ice stress anomaly along the shelf break and offshore (Figures 1a and 1b), which is a known response of the CMIP models to high greenhouse gases concentrations by 2100 (Goyal et al., 2021; Holland et al., 2019; Swart & Fyfe, 2012). We also find an increased westward stress along most of the ice sheet margin (Figure 1b), which is possibly related to higher air temperature gradient across the ice-sheet–ocean boundary in the presence of reduced sea ice cover in the future. On average over the continental shelf, the Ekman downward velocity due to the wind and sea ice stress is weakened by 50% in the future compared to present day (Section S2 in Supporting Information S1).

In terms of surface heat fluxes, the Amundsen continental shelf loses 41% less energy to the atmosphere in the future compared to present-day (Figures 1c and 1d), which is consistent with the effect of a warmer troposphere on downward sensible and longwave heat fluxes over the open ocean and sea ice. Precipitation increases by 22% (Figures 1e and 1f) due to a higher water holding capacity of the troposphere in a warmer climate (Donat-Magnin et al., 2021). The increased precipitation and the reduced sea ice production over the continental shelf (from 0.23 to 0.19 Gt yr$^{-1}$) are together responsible for an annual rate of surface buoyancy loss reduced by 75% in the future compared to present day (Section S2 in Supporting Information S1).

We adopt a similar approach for the lateral boundaries of our regional ocean–sea-ice simulations and add the CMIP5 multi-model mean seasonal anomalies to the present-day lateral boundary conditions (for temperature, salinity, ocean velocity, sea ice concentration, sea ice thickness, and snow-on-ice thickness). The perturbation applied at our lateral boundaries is comprehensively described in Section S3 in Supporting Information S1, which can be summarized as a warming that exceeds 0.25°C everywhere in the first 1,000 m and reaches 2°C in the northernmost part of our domain, as well as a freshening of the first 100 m that is particularly pronounced near the Antarctic coast.

Two additional sensitivity experiments are performed for further insight into the processes. First, we repeat the future simulation of ensemble member B but we only apply the future surface forcing, that is, we keep the present-day lateral boundary conditions for ocean and sea ice. Second, we repeat the future simulation of ensemble member C but with increased iceberg melting (which is kept at present-day values in the other experiments). Following the calculations presented in Section S4 in Supporting Information S1, we increase the total iceberg melt flux over the Amundsen continental shelf from 63 Gt yr$^{-1}$ at present-day to 136 Gt yr$^{-1}$ at the end of the 21st century under RCP8.5 (Figures 1g and 1h).

## 3. Results: Changes in Ice Shelf Basal Melting and Related Processes

On average over the three ensemble members, the ice shelf melt rates are multiplied by 1.4–2.2 (depending on the ice shelf) from present day to future (Figure 2a). The total ice shelf meltwater flux in the Amundsen Sea increases by 346 Gt yr$^{-1}$ on average (Figures 2b and 2c), with a standard deviation of 54 Gt yr$^{-1}$ across the ensemble.

Interestingly, members B and C give almost identical future melt rates while present-day values differ significantly (Figure 2a). As the only difference between B and C is the set of sea ice parameters, this indicates that sea ice production and the related surface buoyancy flux are important drivers of ice shelf melting presently, but no longer play a role in the future. This is very likely related to both the 75% reduction of the surface buoyancy loss in the future and the mixing of more ice shelf meltwater into the surface layer. Both increase the ocean stratification and prevent surface waters from reaching deeper warmer layers on the continental shelf through convective mixing. We also do not find any significant difference between projection C with and without increased iceberg melt rates (not shown), which supports the idea of a decoupling between the surface and the deeper layers in the future.

The changes in melt rates for member B without perturbations of NEMO's lateral boundaries are shown by the white disruption of the middle brown bars in Figure 2a. Increased melt rates underneath Abbot and Venable ice
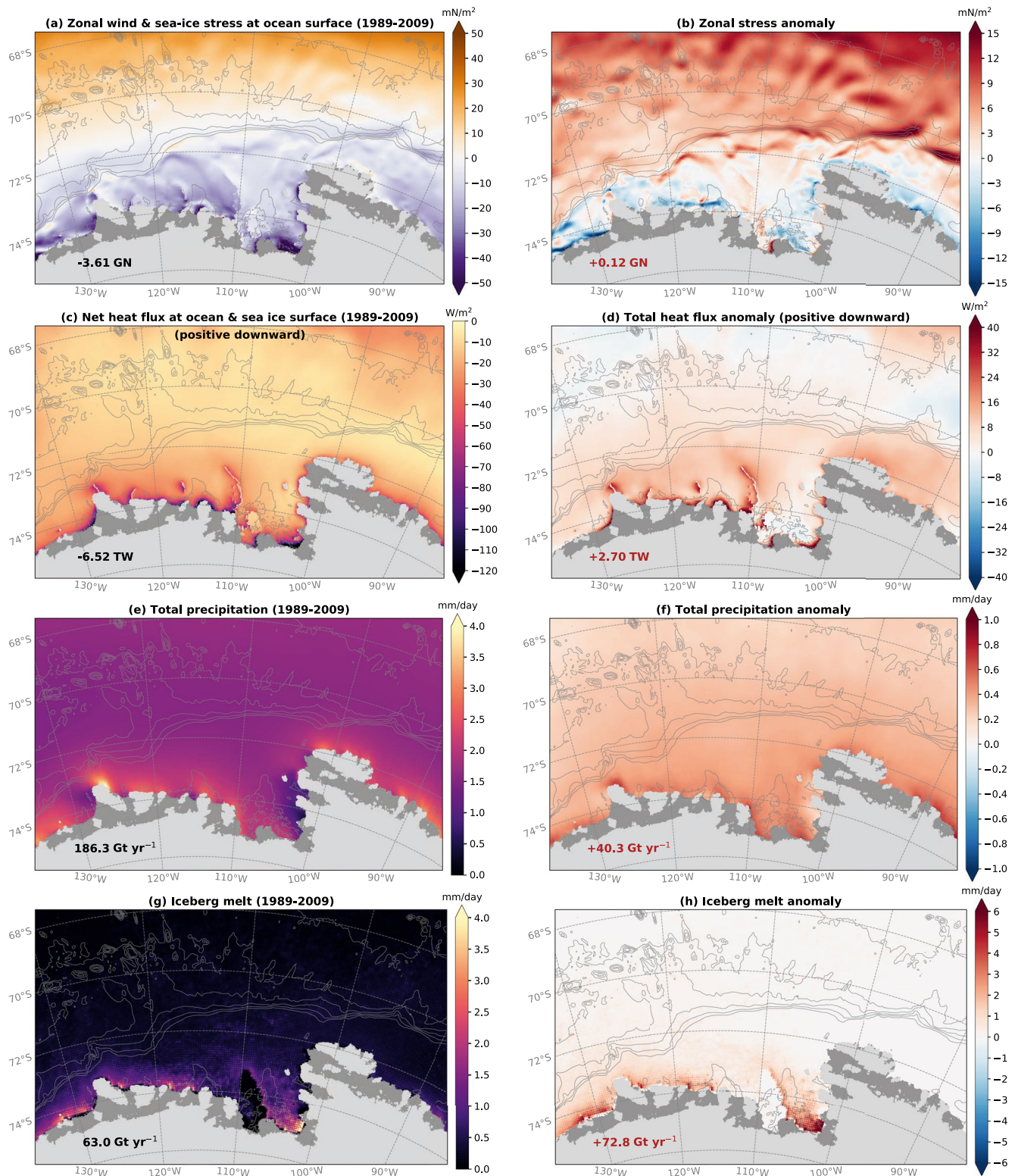
**Figure 1.** Present-day atmospheric forcing (left) and future anomalies with respect to present day (right). Anomalies are calculated as the average of 2080–2100 minus 1989–2009. The grounded ice sheet and the ice shelves are shaded in light and dark gray, respectively. The gray contours indicate the bathymetry (every 750 m). Numbers near the lower left corner indicate the value of the plotted field integrated over the continental shelf, which is defined as the area between the 1500 m isobath and the coastline, and between 100°W and 135°W.

**Figure 2.** (a) Mean present day and future melt rates of individual ice shelves in model configurations A, B, and C (in meters of liquid wate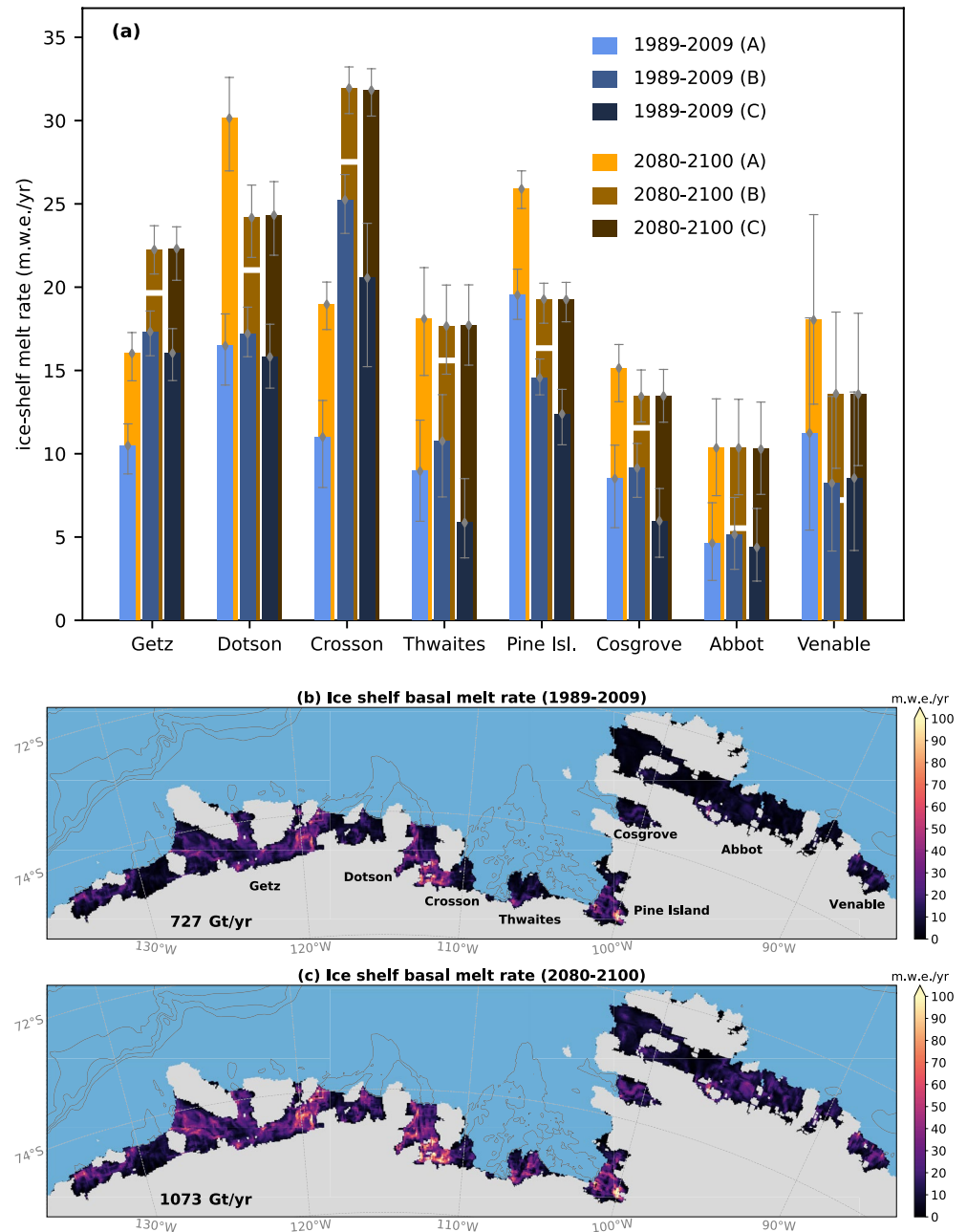r equivalent per year, i.e., $10^3 \ kg \ m^{-2} \ yr^{-1}$). The gray bars cover 95% of the monthly values, that is, between the 2.5th and the 97.5th percentiles. The white disruption of the light brown bars (B over 2080–2100) represent the future melt rate in the experiment with lateral boundary conditions kept at present-day values. (b), (c) Present-day and future ice shelf melt rates, and integrated value over the domain in the lower left corner. The black contours indicate the bathymetry (every 750 m).

shelves are almost entirely explained by the modified lateral boundary conditions. For the other ice shelves, the part of increased melt rate attributed to the lateral boundaries varies from 1/3 to 2/3 of the total change, depending on the ice shelf. This indicates that future changes in remote ocean properties are important, that is, local changes in the atmospheric forcing cannot entirely explain the projected increase in ice shelf melt rates.

We then use the terms of the exact heat and salt budget (saved online and calculated as in Jourdain et al., 2017) to get further insights into the physical mechanisms. The offshore projection is characterized by a 0.25°C warming

below the thermocline due to horizontal advection from the domain boundaries, a 75 m higher thermocline explained by horizontal advection and decreased convective mixing due to less sea ice formation, and a surface freshened by 0.4 g kg$^{-1}$ (Fig. S6 and its description in Section S4 of Supporting Information S1). Changes over the continental shelf are more intense, with 0.5°C warming at depth, a 160 m higher thermocline (Figure 3a), and surface freshened by 0.5 g kg$^{-1}$ (Figure 3b). In contrast to the offshore mechanisms, vertical advection plays a key role on the continental shelf (Figures 3c and 3d). Approximately half of the heat brought by changes in vertical advection between 250 and 800 m is due to the melt-induced circulation in ice shelf cavities and is mostly consumed as latent heat for ice melting (compare Figures 3c and 3d and Figures 3e and 3f). The remaining part is consistent with the reduced Ekman downwelling described in the previous section and in Spence et al. (2014) and Naughten et al. (2022), which reduces the downward advection of relatively cold and fresh water from the top 250 m layer to deeper layers (Figures 3c and 3d). A closer look at the budget terms within ice shelf cavities (not shown) reveals an additional input of heat and freshwater between 100 and 400 m depth corresponding to the melt-induced circulation that releases a mixture of meltwater and entrained Circumpolar Deep Water (CDW) at the ice shelf front as described by Jourdain et al. (2017).

Given the importance of stratification, it is worth discussing the freshening sources in the top 250 m. Out of the 346 Gt yr$^{-1}$ of additional ice shelf meltwater, 51 Gt yr$^{-1}$ are injected directly into the top 250 m layer, which is of comparable magnitude as the 73 Gt yr$^{-1}$ of increased iceberg melting (Figure 1h), 40 Gt yr$^{-1}$ of increased precipitation (Figure 1f), and a sea ice production decreased by 37 Gt yr$^{-1}$ which is equivalent to a freshwater release of 30 Gt yr$^{-1}$ (for a sea ice salinity of 6.3 g kg$^{-1}$). Together, these contributions are responsible for a salinity decrease of $-1.20$ g kg$^{-1}$ on average in the top 250 m (Figure 3d). Vertical advection is responsible for an additional decrease of $-1.33$ g kg$^{-1}$, while horizontal advection compensates a large part of these two freshening contributions. Without specific tracer experiments, it is difficult to robustly associate the freshening effect of vertical advection with ice shelf meltwater produced deeper than 250 m. Nonetheless, given that $-1.20$ g kg$^{-1}$ was induced by $+194$ Gt yr$^{-1}$ of direct freshwater flux into the top 250 m, the 295 Gt yr$^{-1}$ of ice shelf meltwater produced below 250 m would be expected to decrease salinity by $-1.84$ g kg$^{-1}$ if the meltwater were entirely transported into the top 250 m. Therefore, this suggests that either only 72% of the ice shelf meltwater produced below 250 m has been advected into the top 250 m, or the melt-induced circulation has transported a mix of fresh meltwater and salty CDW into the top 250 m, as previously shown by Jourdain et al. (2017).

## 4. Results: Assessment of Simple Ice Shelf Melt Parameterizations

Here we use our NEMO projections to assess the non-local (also referred to as semi-local) quadratic parameterization proposed by Favier et al. (2019) and used in some of the standard ice sheet projections of the Ice Sheet Model Intercomparison Project for CMIP6 (ISMIP6, Nowicki et al., 2020; Seroussi et al., 2020), with a melt rate defined as:

$$m(x, y) = K \times (TF(x, y, z_{\text{draft}}) + \delta T) \times |\langle TF \rangle_{\text{ice-shelf}} + \delta T| \tag{1}$$

where $TF(x, y, z_{\text{draft}})$ is the thermal forcing at the ice-ocean interface of depth $z_{\text{draft}}$, and $\langle TF \rangle_{\text{ice-shelf}}$ the thermal forcing averaged over an entire ice shelf draft. The temperature correction $\delta T$ is used to correct biases in present-day observations and to account for melt-induced cooling or other poorly represented processes (Jourdain et al., 2020). $K$ is a tuning coefficient that was expressed in various ways across previous studies. An expression of $K$ was proposed by Favier et al. (2019) and Jourdain et al. (2020), but we find the expression proposed by Jenkins et al. (2018) and Burgard et al. (2022) more physically sound. For ISMIP6, Jourdain et al. (2020) proposed two calibration methods, one referred to as "MeanAnt," ensuring realistic present-day melt rates at the scale of Antarctica for minimal temperature corrections and giving $K_{\text{MeanAnt}} = 2.57$ m yr$^{-1}$ K$^{-2}$, and the other one referred to as "PIGL", ensuring more realistic present-day melt rates near Pine Island's grounding line and giving $K_{\text{PIGL}} = 28.2$ m yr$^{-1}$ K$^{-2}$, but requiring negative $\delta T$ corrections almost everywhere to keep reasonable melt rates for individual ice shelves or integrated over larger sectors.

In the following, we assume that the present-day temperature is perfectly known, so that we can use $\delta T = 0$ for MeanAnt and we find that present-day RMSE from PIGL are lowest for $\delta T = -1.9$°C. For clarity, we just show the results for Pine Island and Thwaites (Figure 4), which are key ice shelves for the Antarctic contribution to sea level rise, but the other ice shelves have a very similar behavior. We estimate the future parameterized melt rates in two ways: (1) from the future ocean temperatures simulated by NEMO (orange dashed curves in Figure 4), and
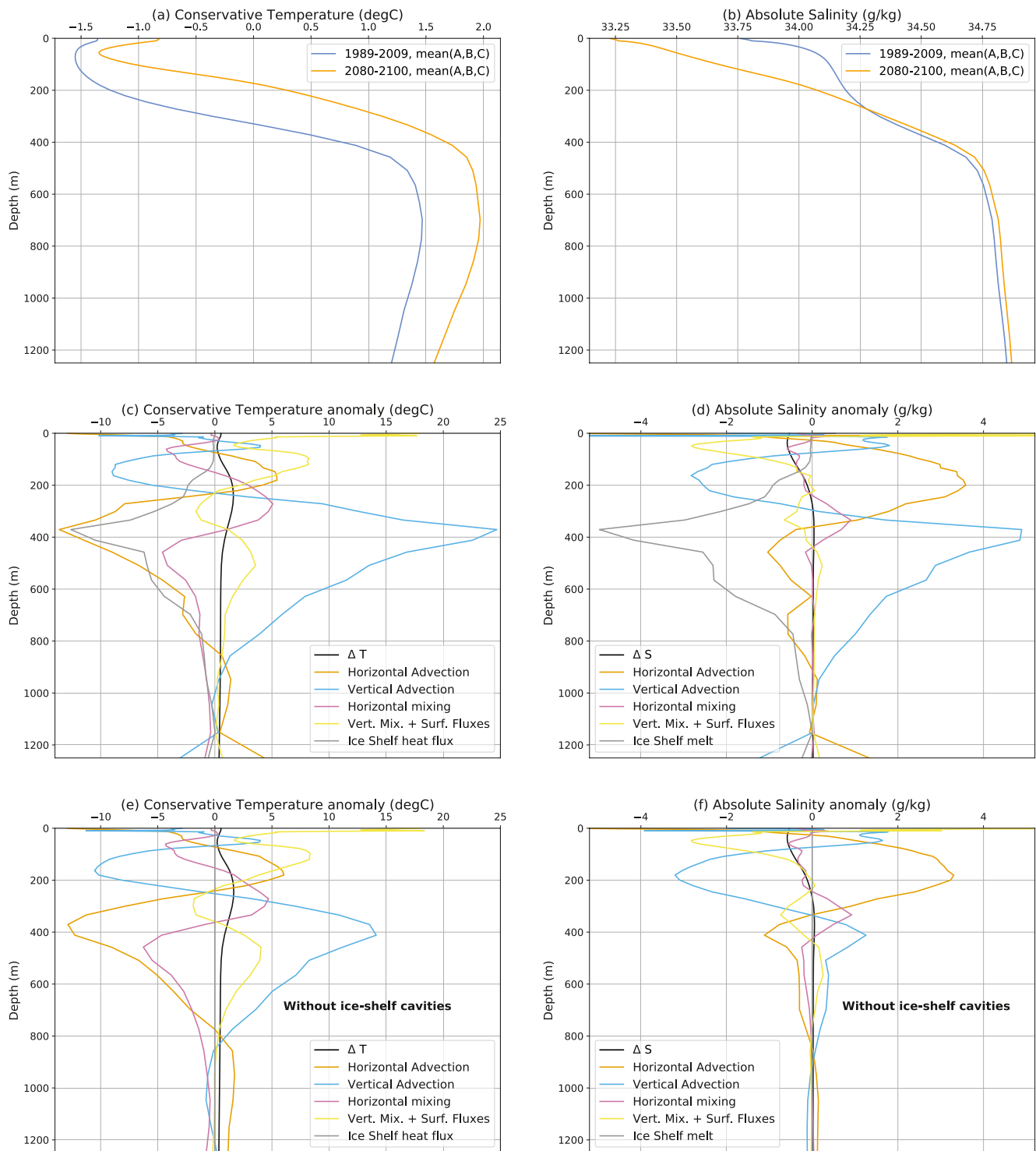
**Figure 3.** (a),(b) Present-day and future conservative temperature and absolute salinity profiles over the Amundsen Sea continental shelf (defined as the area between the 1500 m isobath and the coastline, and between 100°W and 135°W), including ice shelf cavities. (c),(d) temperature (ΔT) and salinity (ΔS) change from present-day to future conditions and contributions of the individual terms of the heat and salt equations to ΔT and ΔS, respectively. The individual tendency terms of the heat and salt equations were integrated in time from the initial state until each month of either 1989–2009 or 2080–2100, then averaged over each of these 20-year periods, from which we extracted the difference between the two periods (similar to equations 6 and 7 of Jourdain et al., 2017). (e),(f) same as (c),(d) but excluding ice shelf cavities from the heat and salt budget calculation.
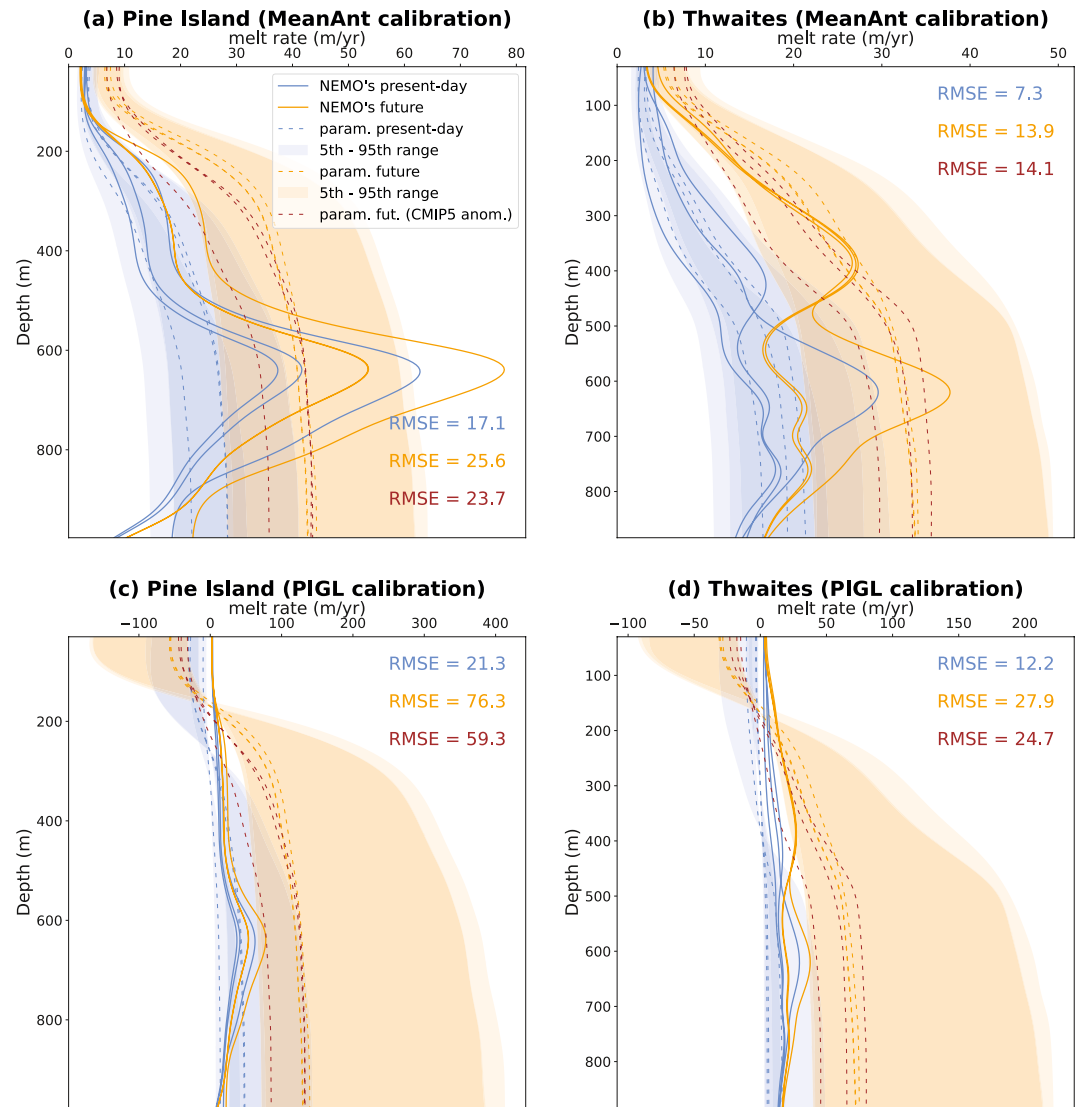
**Figure 4.** Melt profiles beneath Pine Island (left) and Thwaites (right) ice shelves, from the NEMO simulations (solid lines), and from the ISMIP6 standard parameterization (dashed lines) tuned following either the "MeanAnt" (upper panels) or the "PIGL" (lower panels) method (median $K$ coefficient derived from Jourdain et al., 2020). The present day parameterized melt rates are based on NEMO's present-day temperatures in front of the ice shelf cavities (within 50 km from the ice shelf front). The future melt rate is either calculated from the's future temperatures simulated by NEMO (orange dashed lines) or from the CMIP5 multi-model mean temperature anomaly (dark red dashed lines). The semi-transparent shaded areas indicate the range corresponding to the 5th and 95th percentiles of $K$ coefficients based on the future temperatures produced by NEMO (values derived from Tab. 2 of Jourdain et al., 2020). The three curves for each estimate correspond to the three members of our small ensemble. Every curve is built using a kernel density estimate based on a Gaussian function of standard deviation equal to 1/20th of the maximum ice draft depth. The Root Mean Square Errors (RMSE, in m/yr) are calculated for the spatial pattern with regards to the NEMO values and correspond to the median $K$ values.

(2) from the CMIP5 multi-model mean ocean warming added to the NEMO present-day temperatures (dashed dark red curves in Figure 4), which corresponds to what is commonly used in standalone ice sheet projections like ISMIP6.

First of all, the present-day parameterized melt rates overall agree with NEMO although the exact vertical distribution is only poorly captured (blue curves in Figure 4). The MeanAnt curves show some overlap between the three model projections and the 90th confidence interval of the parameterized projections (orange curves in Figures 4a and 4b), although the RMSE approximately doubles compared to present day. The PIGL projections are much worse, with very little overlap between the three model projections and the 90th confidence interval of

the parameterized projections (orange curves in Figures 4c and 4d). For the 95th percentile of $K$, the maximum melt rates in either Pine Island or Thwaites cavity are overestimated by a factor of five. The melt projections directly based on the CMIP5 ocean warming (dashed dark red curves in Figure 4) are similar to the projections from the warming produced by NEMO, indicating that most of the bias comes from the parameterization itself.

## 5. Discussion and Conclusion

In this paper, we have built an ensemble of three 1/12° ocean–sea-ice–ice-shelf projections of the late 21st century under the RCP8.5 concentration pathway. In these simulations, the net surface buoyancy loss is reduced by 75% in the future compared to present day due to surface freshening by increased precipitation, increased iceberg melt and reduced sea ice production. Increased ice shelf melt also contributes greatly to making the surface layer fresher and more buoyant in the future. The result is a decoupling between the surface layer and deeper layers on the continental shelf, which makes future ice shelf melt insensitive to additional perturbations of surface buoyancy fluxes. We find that the future Ekman downwelling velocity is reduced by half over the continental shelf compared to present day. This, in addition to the melt-induced circulation, largely explains the additional heat made available to ice shelf melting. However, regional changes in atmospheric forcing only explain 1/3 to 2/3 of the increase in ice shelf melt rates (depending on the ice shelf). The remaining is due to advection of warmer water from remote locations (i.e., from our model domain lateral boundaries). The importance of advection from remote locations was already evidenced by Nakayama et al. (2018) for the interannual variability of the Amundsen Sea. Here we clearly show the caveats of attributing future changes in ice shelf melting to regional atmospheric perturbations in the Amundsen Sea (e.g., Holland et al., 2019).

The relative changes in melt rates (+48% for all simulated ice shelves, Figures 2b and 2c) are lower than previous estimates, for example, +189% until 2100 in the Amundsen Sea for the CMIP5 multi-model mean under RCP8.5 in Naughten, Meissner, Galton-Fenzi, England, Timmermann, and Hellmer (2018) and +250% until 2100 for Pine Island under the A1B and E1 scenarios in Timmermann and Hellmer (2013). The present-day melt rates were strongly underestimated in these previous studies, due to a cold bias on the continental shelf. Such a cold Amundsen Sea is very sensitive to changes in surface heat and buoyancy fluxes that can induce a transition from sea-floor temperatures near the surface freezing point to much warmer conditions typical of the presence of CDW. In our case, we start from a more realistic state with weakly modified CDW on the continental shelf, so that important warming at depth is unlikely to be triggered by reasonable changes in the surface, and the Ekman dynamics is more likely the main driver of changes in ice shelf melt rates. We nonetheless acknowledge that our 0.5°C warm bias may lead to an underestimation of present-day episodic convection, leading to an underestimation of the ocean warming and relative increase in ice shelf melt rates. For a given ocean warming, starting from cold biased conditions also produces important relative changes in melt rates because the calculation of relative change involves a division by the initial thermal forcing. For example, assuming a quadratic dependency of melt to the thermal forcing (Holland et al., 2008), 0.5°C of future warming at 600 m depth would correspond to melt rates increased by 143% starting from the −2.6°C bias of Naughten, Meissner, Galton-Fenzi, England, Timmermann, and Hellmer (2018), by 30% starting from an observed temperature of 1.0°C (Dutrieux et al., 2014) and by 26% (starting from our simulations with a +0.5°C bias).

Our projection method is innovative in the sense that it enables a representation of the CMIP multi-model mean at relatively high resolution and with basic bias correction. We have chosen to drive our projections directly by the CMIP multi-model mean because it is often considered as the best estimate for future climate as individual model biases are partly canceled (Knutti et al., 2010). The use of future anomalies with respect to present day is expected to remove a part of the biases in individual model projections given that the CMIP model biases are largely stationary even under strong climate changes (Krinner & Flanner, 2018), while conserving linearities like the geostrophic balance. Besides, the numerical cost of each 1/12° ocean simulation precludes forcing them by each of the 33 CMIP5 models for both present and future conditions. However, an important limitation of our projection method is that we do not account for possible changes in the frequency of interannual events like El Niño (Cai et al., 2014), and it will be important to confront our results to direct downscaling of the CMIP models. Finally, we have chosen to force our ocean simulations using a 10 km regional atmospheric model, which is expected to be more realistic along the coastline and the shelf break than the much coarser CMIP models (e.g., Dinniman et al., 2015; Huot et al., 2021), although the use of such an intermediate model may be an additional source of biases and uncertainty in the chain of projections. The regional atmosphere model (MAR) is

nonetheless renowned for its representation of polar processes in the Antarctic coastal region (e.g., Donat-Magnin et al., 2020; Kittel et al., 2022; Mottram et al., 2021), while most CMIP models have representations of snow, clouds and surface boundary layers that are less accurate in polar regions (e.g., Lenaerts et al., 2016; Lenaerts et al., 2017). Yet, it will be important to explore other projection methods to confirm the results of this study.

All our conclusions are nonetheless based on a single ocean model, even if we used three different set-ups, and it will be important to challenge these results using different ocean models. Our 1/12° resolution enables the resolution of eddies in the Southern Ocean, which is key to simulating future sea ice decline (Rackow et al., 2022) and future heat transport toward Antarctica (van Westen & Dijkstra, 2021). This resolution is also sufficient for the resolution of mean flow topography interactions involved in bringing CDW onto the continental shelf (St-Laurent et al., 2013), but not sufficient to resolve eddies on the continental shelf and within ice shelf cavities (Stewart et al., 2018), or the interaction between Rossby waves along the shelf break and bathymetric troughs (St-Laurent et al., 2013). It remains difficult to estimate the contribution of these small scales to the future evolution of heat transport toward the ice shelf cavities of the Amundsen Sea as previous high-resolution estimates of this contribution did not represent fine-scale bathymetry and ice shelf cavities in the Amundsen Sea (Stewart et al., 2018). Another important limitation of our modeling approach is that there is no ice sheet model coupled to NEMO in this study, that is, ice shelves are static. This was shown to be an important limitation (Donat-Magnin et al., 2017), albeit for much stronger and longer melt perturbations.

Finally, given that the Antarctic Ice Sheet projections show the highest sensitivity to increased basal melt rates in the Amundsen Sea sector (Seroussi et al., 2020), our regional results can provide a critical perspective on the Antarctic contribution to the 21st century sea level rise simulated within ISMIP6 (Seroussi et al., 2020) and emulated by Edwards et al. (2021). The high-end estimates for 2100 under RCP8.5 (∼30 cm of additional sea level) were obtained from the 95th percentile of the PIGL parameters, which we find highly incompatible with our simulations. Edwards et al. (2021) empirically defined a continuous distribution of $K$ coefficients (their Figure 3d), with a relatively large cumulative probability around the median PIGL parameter, and low-probability extreme values beyond the 95th percentile of PIGL parameters. Our projections suggest that this distribution should be narrowed toward lower values and that lower parameters should be used even for risk averse projections.

## Data Availability Statement

The model version and set of parameters used to run our experiments are provided in https://doi.org/10.5281/zenodo.6644859. The main model outputs (climatological values) are provided in https://doi.org/10.5281/zenodo.7225758. All the python scripts used to build the figures are provided in https://doi.org/10.5281/zenodo.7224252 and are mainly based on the Xarray (Hoyer & Hamman, 2017), Numpy (Harris et al., 2020) and Matplotlib (Hunter, 2007) packages.

## References

Asay-Davis, X. S., Jourdain, N. C., & Nakayama, Y. (2017). Developments in simulating and parameterizing interactions between the Southern Ocean and the Antarctic ice sheet. *Current Climate Change Reports*, *3*(4), 316–329. https://doi.org/10.1007/s40641-017-0071-0

Bett, D. T., Holland, P. R., Naveira Garabato, A. C., Jenkins, A., Dutrieux, P., Kimura, S., & Fleming, A. (2020). The impact of the Amundsen Sea freshwater balance on ocean melting of the West Antarctic Ice Sheet. *Journal of Geophysical Research: Oceans*, *125*(9), e2020JC016305. https://doi.org/10.1029/2020jc016305

Budge, J. S., & Long, D. G. (2018). A comprehensive database for Antarctic iceberg tracking using scatterometer data. *IEEE Journal of Selected Topics in Applied Earth Observations and Remote Sensing*, *11*(2), 434–442. https://doi.org/10.1109/jstars.2017.2784186

Burgard, C., Jourdain, N. C., Reese, R., Jenkins, A., & Mathiot, P. (2022). *An Assessment of Basal Melt Parameterisations for Antarctic Ice Shelves*. The Cryosphere Discussion.

Cai, W., Borlace, S., Lengaigne, M., Van Rensch, P., Collins, M., Vecchi, G., et al. (2014). Increasing frequency of extreme El Niño events due to greenhouse warming. *Nature Climate Change*, *4*(2), 111–116. https://doi.org/10.1038/nclimate2100

DeConto, R. M., Pollard, D., Alley, R. B., Velicogna, I., Gasson, E., Gomez, N., et al. (2021). The Paris Climate Agreement and future sea-level rise from Antarctica. *Nature*, *593*(7857), 83–89. https://doi.org/10.1038/s41586-021-03427-0

Dinniman, M. S., Klinck, J. M., Bai, L.-S., Bromwich, D. H., Hines, K. M., & Holland, D. M. (2015). The effect of atmospheric forcing resolution on delivery of ocean heat to the Antarctic floating ice shelves. *Journal of Climate*, *28*(15), 6067–6085. https://doi.org/10.1175/jcli-d-14-00374.1

Donat-Magnin, M., Jourdain, N. C., Gallée, H., Amory, C., Kittel, C., Fettweis, X., et al., (2020). Interannual variability of summer surface mass balance and surface melting in the Amundsen sector, west Antarctica. *The Cryosphere*, *14*(1), 229–249. https://doi.org/10.5194/tc-14-229-2020

Donat-Magnin, M., Jourdain, N. C., Kittel, C., Agosta, C., Amory, C., Gallée, H., et al. (2021). Future surface mass balance and surface melt in the Amundsen sector of the West Antarctic Ice Sheet. *The Cryosphere*, *15*(2), 571–593. https://doi.org/10.5194/tc-15-571-2021

Donat-Magnin, M., Jourdain, N. C., Spence, P., Le Sommer, J., Gallée, H., & Durand, G. (2017). Ice-shelf melt response to changing winds and glacier dynamics in the Amundsen Sea sector, Antarctica. *Journal of Geophysical Research*, *122*(12), 10206–10224.

Durand, G., van den Broeke, M. R., Le Cozannet, G., Edwards, T. L., Holland, P. R., Jourdain, N. C., et al. (2022). Sea-level rise: From global perspectives to local services. *Frontiers in Marine Science*, 2088.

Dutrieux, P., De Rydt, J., Jenkins, A., Holland, P. R., Ha, H. K., Lee, S. H., et al. (2014). Strong sensitivity of Pine Island ice-shelf melting to climatic variability. *Science*, *343*(6167), 174–178. https://doi.org/10.1126/science.1244341

Edwards, T. L., Nowicki, S., Marzeion, B., Hock, R., Goelzer, H., Seroussi, H., et al. (2021). Projected land ice contributions to twenty-first-century sea level rise. *Nature*, *593*(7857), 74–82.

Eyring, V., Bony, S., Meehl, G. A., Senior, C. A., Stevens, B., Stouffer, R. J., & Taylor, K. E. (2016). Overview of the coupled model intercomparison Project Phase 6 (CMIP6) experimental design and organization. *Geoscientific Model Development*, *9*(5), 1937–1958. https://doi.org/10.5194/gmd-9-1937-2016

Favier, L., Jourdain, N. C., Jenkins, A., Merino, N., Durand, G., Gagliardini, O., et al. (2019). Assessment of sub-shelf melting parameterisations using the ocean-ice sheet coupled model NEMO (v3. 6)-Elmer/Ice (v8. 3). *Geoscientific Model Development*. https://doi.org/10.5194/gmd-12-2255-2019

Fox-Kemper, B., Hewitt, H., Xiao, C., Aalgeirsdóttir, G., Drijfhout, S. S., Edwards, T. L., et al. (2021). Ocean, cryosphere and sea level change. In *Climate change 2021: The physical Science Basis. Contribution of working Group I to the Sixth Assessment Report of the Intergovernmental panel on climate change* (pp. 1211–1362). Cambridge University Press. https://doi.org/10.1017/9781009157896.011

Gallée, H., & Schayes, G. (1994). Development of a three-dimensional meso-$\gamma$ primitive equation model: Katabatic winds simulation in the area of Terra Nova Bay, Antarctica. *Monthly Weather Review*, *122*(4), 671–685. https://doi.org/10.1175/1520-0493(1994)122<0671:doatdm>2.0.co;2

Goyal, R., Sen Gupta, A., Jucker, M., & England, M. H. (2021). Historical and projected changes in the southern hemisphere surface westerlies. *Geophysical Research Letters*, *48*(4), e2020GL090849. https://doi.org/10.1029/2020gl090849

Harris, C. R., Millman, K. J., van der Walt, S. J., Gommers, R., Virtanen, P., Cournapeau, D., et al. (2020). Array programming with NumPy. *Nature*, *585*(7825), 357–362. https://doi.org/10.1038/s41586-020-2649-2

Hausfather, Z., & Peters, G. P. (2020a). Emissions the business as usual'story is misleading. *Nature*, *577*(7792), 618–620. https://doi.org/10.1038/d41586-020-00177-3

Hausfather, Z., & Peters, G. P. (2020b). RCP8. 5 is a problematic scenario for near-term emissions. *Proceedings of the National Academy of Sciences of the United States of America*, *117*(45), 27791–27792. https://doi.org/10.1073/pnas.2017124117

Hinkel, J., Church, J. A., Gregory, J. M., Lambert, E., Le Cozannet, G., Lowe, J., et al. (2019). Meeting user needs for sea level rise information: A decision analysis perspective. *Earth's Future*, *7*(3), 320–337. https://doi.org/10.1029/2018ef001071

Holland, P. R., Bracegirdle, T. J., Dutrieux, P., Jenkins, A., & Steig, E. J. (2019). West Antarctic ice loss influenced by internal climate variability and anthropogenic forcing. *Nature Geoscience*, 1–7. https://doi.org/10.1038/s41561-019-0420-9

Holland, P. R., Jenkins, A., & Holland, D. M. (2008). The response of ice shelf basal melting to variations in ocean temperature. *J. Climate*, *21*(11), 2558–2572. https://doi.org/10.1175/2007jcli1909.1

Hoyer, S., & Hamman, J. (2017). xarray: N-D labeled arrays and datasets in Python. *Journal of Open Research Software*, *5*(1). https://doi.org/10.5334/jors.148

Hunter, J. D. (2007). Matplotlib: A 2D graphics environment. *Computing in Science & Engineering*, *9*(3), 90–95. https://doi.org/10.1109/MCSE.2007.55

Huot, P.-V., Kittel, C., Fichefet, T., Jourdain, N. C., Sterlin, J., & Fettweis, X. (2021). Effects of the atmospheric forcing resolution on simulated sea ice and polynyas off Adélie Land, East Antarctica. *Ocean Modelling*, *168*, 101901. https://doi.org/10.1016/j.ocemod.2021.101901

Jenkins, A., Shoosmith, D., Dutrieux, P., Jacobs, S., Kim, T. W., Lee, S. H., et al. (2018). West Antarctic Ice Sheet retreat in the Amundsen Sea driven by decadal oceanic variability. *Nature Geoscience*, *11*, 733–738. https://doi.org/10.1038/s41561-018-0207-4

Jourdain, N. C., Asay-Davis, X., Hattermann, T., Straneo, F., Seroussi, H., Little, C. M., & Nowicki, S. (2020). A protocol for calculating basal melt rates in the ISMIP6 Antarctic ice sheet projections. *The Cryosphere*, *14*(9), 3111–3134. https://doi.org/10.5194/tc-14-3111-2020

Jourdain, N. C., Mathiot, P., Merino, N., Durand, G., Le Sommer, J., Spence, P., et al. (2017). Ocean circulation and sea-ice thinning induced by melting ice shelves in the Amundsen Sea. *Journal of Geophysical Research: Oceans*, *122*(3), 2550–2573. https://doi.org/10.1002/2016jc012509

Jourdain, N. C., Merino, N., Le Sommer, J., Durand, G., & Mathiot, P. (2019). *Interannual Iceberg meltwater fluxes over the Southern Ocean (1.0)* (Technical Report). https://doi.org/10.5281/zenodo.3514728

Jourdain, N. C., Molines, J.-M., Le Sommer, J., Mathiot, P., Chanut, J., de Lavergne, C., & Madec, G. (2019). Simulating or prescribing the influence of tides on the Amundsen Sea ice shelves. *Ocean Modelling*, *133*, 44–55. https://doi.org/10.1016/j.ocemod.2018.11.001

Kittel, C., Amory, C., Hofer, S., Agosta, C., Jourdain, N. C., Gilbert, E., et al. (2022). Clouds drive differences in future surface melt over the Antarctic ice shelves. *The Cryosphere*, *16*(7), 2655–2669. https://doi.org/10.5194/tc-16-2655-2022

Knutti, R., Furrer, R., Tebaldi, C., Cermak, J., & Meehl, G. A. (2010). Challenges in combining projections from multiple climate models. *Journal of Climate*, *23*(10), 2739–2758. https://doi.org/10.1175/2009jcli3361.1

Krinner, G., & Flanner, M. G. (2018). Striking stationarity of large-scale climate model bias patterns under strong climate change. *Proceedings of the National Academy of Sciences*, *115*(38), 9462–9466. https://doi.org/10.1073/pnas.1807912115

Lenaerts, J. T. M., Van Tricht, K., Lhermitte, S., & L'Ecuyer, T. S. (2017). Polar clouds and radiation in satellite observations, reanalyses, and climate models. *Geophysical Research Letters*, *44*(7), 3355–3364. https://doi.org/10.1002/2016gl072242

Lenaerts, J. T. M., Vizcaino, M., Fyke, J., Van Kampenhout, L., & van den Broeke, M. R. (2016). Present-day and future Antarctic ice sheet climate and surface mass balance in the Community Earth System Model. *Climate Dynamics*, *47*(5–6), 1367–1381. https://doi.org/10.1007/s00382-015-2907-4

Levermann, A., Winkelmann, R., Albrecht, T., Goelzer, H., Golledge, N. R., Greve, R., et al. (2020). Projecting Antarctica's contribution to future sea level rise from basal ice shelf melt using linear response functions of 16 ice sheet models (LARMIP-2). *Earth System Dynamics*, *11*(1), 35–76. https://doi.org/10.5194/esd-11-35-2020

Madec, G., & NEMO-Team. (2016). Note du Pôle de modélisation de l'Institut Pierre-Simon Laplace No 27, ISSN No. 1288-1619. In *NEMO Ocean Engine, Version 3.6 Stable (Technical Report)*. France: IPSL.

Mathiot, P., Jenkins, A., Harris, C., & Madec, G. (2017). Explicit and parametrised representation of under ice shelf seas in az* coordinate ocean model NEMO 3.6. *Geoscientific Model Development*, *10*(7), 2849–2874. https://doi.org/10.5194/gmd-10-2849-2017

Merino, N., Jourdain, N. C., Le Sommer, J., Goosse, H., Mathiot, P., & Durand, G. (2018). Impact of increasing Antarctic glacial freshwater release on regional sea-ice cover in the Southern Ocean. *Ocean Modelling*, *121*, 76–89. https://doi.org/10.1016/j.ocemod.2017.11.009

Merino, N., Le Sommer, J., Durand, G., Jourdain, N. C., Madec, G., Mathiot, P., & Tournadre, J. (2016). Antarctic icebergs melt over the Southern Ocean: Climatology and impact on sea-ice. *Ocean Modelling*, *104*, 99–110. https://doi.org/10.1016/j.ocemod.2016.05.001

Morlighem, M. (2020). MEaSUREs BedMachine Antarctica, Version 2 (Technical Report). *Boulder, CO: NASA National Snow and Ice Data Center Distributed Active Archive Center*. Retrieved from https://nsidc.org/data/NSIDC-0756/versions/2 https://doi.org/10.5067/E1QL9HFQ7A8M

Morlighem, M., Rignot, E., Binder, T., Blankenship, D., Drews, R., Eagles, G., et al. (2020). Deep glacial troughs and stabilizing ridges unveiled beneath the margins of the Antarctic ice sheet. *Nature Geoscience*, *13*(2), 132–137. https://doi.org/10.1038/s41561-019-0510-8

Mottram, R., Hansen, N., Kittel, C., van Wessem, J. M., Agosta, C., Amory, C., et al. (2021). What is the surface mass balance of Antarctica? An intercomparison of regional climate model estimates. *The Cryosphere*, *15*(8), 3751–3784. https://doi.org/10.5194/tc-15-3751-2021

Nakayama, Y., Menemenlis, D., Zhang, H., Schodlok, M., & Rignot, E. (2018). Origin of circumpolar deep water intruding onto the Amundsen and Bellingshausen Sea continental shelves. *Nature Communication*, *9*(1), 1–9. https://doi.org/10.1038/s41467-018-05813-1

Nakayama, Y., Timmermann, R., Schröder, M., & Hellmer, H. H. (2014). On the difficulty of modeling Circumpolar Deep Water intrusions onto the Amundsen Sea continental shelf. *Ocean Modelling*, *84*, 26–34. https://doi.org/10.1016/j.ocemod.2014.09.007

Naughten, K. A., Holland, P. R., Dutrieux, P., Kimura, S., Bett, D. T., & Jenkins, A. (2022). Simulated twentieth-century ocean warming in the Amundsen Sea, west Antarctica. *Geophysical Research Letters*, e2021GL094566. https://doi.org/10.1029/2021GL094566

Naughten, K. A., Meissner, K. J., Galton-Fenzi, B. K., England, M. H., Timmermann, R., & Hellmer, H. H. (2018). Future projections of Antarctic ice shelf melting based on CMIP5 scenarios. *Journal of Climate*, *31*(13), 5243–5261. https://doi.org/10.1175/jcli-d-17-0854.1

Nowicki, S., Payne, A., Goelzer, H., Seroussi, H., Lipscomb, W., Abe-Ouchi, A., et al. (2020). Experimental protocol for sea level projections from ISMIP6 standalone ice sheet models. *The Cryosphere*, *14*, 2331–2368. https://doi.org/10.5194/tc-14-2331-2020

Purich, A., & England, M. H. (2021). Historical and future projected warming of Antarctic Shelf Bottom Water in CMIP6 models. *Geophysical Research Letters*, *48*(10), e2021GL092752. https://doi.org/10.1029/2021gl092752

Rackow, T., Danilov, S., Goessling, H. F., Hellmer, H. H., Sein, D. V., Semmler, T., et al. (2022). Delayed Antarctic sea-ice decline in high-resolution climate change simulations. *Nature Communication*, *13*(1), 1–12. https://doi.org/10.1038/s41467-022-28259-y

Rousset, C., Vancoppenolle, M., Madec, G., Fichefet, T., Flavoni, S., Barthélemy, A., et al. (2015). The Louvain-La-Neuve sea ice model LIM3.6: Global and regional capabilities. *Geoscientific Model Development*, *8*(10), 2991–3005.. https://doi.org/10.5194/gmd-8-2991-2015

Seroussi, H., Nowicki, S., Payne, A. J., Goelzer, H., Lipscomb, W. H., Abe-Ouchi, A., et al. (2020). ISMIP6 Antarctica: A multi-model ensemble of the Antarctic ice sheet evolution over the 21st century. *The Cryosphere*, *14*(9), 3033–3070.

Siahaan, A., Smith, R., Holland, P., Jenkins, A., Gregory, J. M., Lee, V., et al. (2021). The Antarctic contribution to 21st century sea-level rise predicted by the UK Earth System Model with an interactive ice sheet. *The Cryosphere Discussions*, 1–42.

Smith, R. S., Mathiot, P., Siahaan, A., Lee, V., Cornford, S. L., Gregory, J. M., et al. (2021). Coupling the UK Earth System Model to dynamic models of the Greenland and Antarctic ice sheets. *Journal of Advances in Modeling Earth Systems*, *13*(10), e2021MS002520. https://doi.org/10.1029/2021ms002520

Spence, P., Griffies, S. M., England, M. H., Hogg, A. M., Saenko, O. A., & Jourdain, N. C. (2014). Rapid subsurface warming and circulation changes of Antarctic coastal waters by poleward shifting winds. *Geophysical Research Letters*, *41*(13), 4601–4610. https://doi.org/10.1002/2014gl060613

Stewart, A. L., Klocker, A., & Menemenlis, D. (2018). Circum-Antarctic shoreward heat transport derived from an Eddy-and tide-resolving simulation. *Geophysical Research Letters*, *45*(2), 834–845. https://doi.org/10.1002/2017GL075677

St-Laurent, P., Klinck, J. M., & Dinniman, M. S. (2013). On the role of coastal troughs in the circulation of warm Circumpolar Deep Water on Antarctic shelves. *Journal of Physical Oceanography*, *43*(1), 51–64. https://doi.org/10.1175/jpo-d-11-0237.1

Swart, N. C., & Fyfe, J. C. (2012). Observed and simulated changes in the Southern Hemisphere surface westerly wind-stress. *Geophysical Research Letters*, *39*(16). https://doi.org/10.1029/2012gl052810

Timmermann, R., & Hellmer, H. H. (2013). Southern Ocean warming and increased ice shelf basal melting in the twenty-first and twenty-second centuries based on coupled ice-ocean finite-element modelling. *Ocean Dynamics*, *63*(9–10), 1011–1026. https://doi.org/10.1007/s10236-013-0642-0

van Westen, R. M., & Dijkstra, H. A. (2021). Ocean eddies strongly affect global mean sea-level projections. *Science Advances*, *7*(15), eabf1674. https://doi.org/10.1126/sciadv.abf1674

Williamson, D. B., Blaker, A. T., & Sinha, B. (2017). Tuning without over-tuning: Parametric uncertainty quantification for the NEMO ocean model. *Geoscientific Model Development*, *10*(4), 1789–1816. https://doi.org/10.5194/gmd-10-1789-2017

## References From the Supporting Information

Adusumilli, S., Fricker, H. A., Medley, B., Padman, L., & Siegfried, M. R. (2020). Interannual variations in meltwater input to the Southern Ocean from Antarctic ice shelves. *Nature Geoscience*, *13*(9), 616–620. https://doi.org/10.1038/s41561-020-0616-z

Depoorter, M. A., Bamber, J. L., Griggs, J. A., Lenaerts, J. T. M., Ligtenberg, S. R. M., van den Broeke, M. R., & Moholdt, G. (2013). Calving fluxes and basal melt rates of Antarctic ice shelves. *Nature*, *502*(7469), 89–92. https://doi.org/10.1038/nature12567

Joughin, I., Shapero, D., Dutrieux, P., & Smith, B. (2021). Ocean-induced melt volume directly paces ice loss from Pine Island Glacier. *Science Advances*, *7*(43), eabi5738. https://doi.org/10.1126/sciadv.abi5738

Little, C. M., & Urban, N. M. (2016). CMIP5 temperature biases and 21st century warming around the Antarctic coast. *Annals of Glaciology*, *57*(73), 69–78. https://doi.org/10.1017/aog.2016.25

Martin, T., & Adcroft, A. (2010). Parameterizing the fresh-water flux from land ice to ocean with interactive icebergs in a coupled climate model. *Ocean Modelling*, *34*(3), 111–124. https://doi.org/10.1016/j.ocemod.2010.05.001

Meijers, A. J., Shuckburgh, E., Bruneau, N., Sallée, J.-B., Bracegirdle, T. J., & Wang, Z. (2012). Representation of the Antarctic Circumpolar Current in the CMIP5 climate models and future changes under warming scenarios. *Journal of Geophysical Research*, *117*(C12). https://doi.org/10.1029/2012jc008412

Naughten, K. A., Meissner, K. J., Galton-Fenzi, B. K., England, M. H., Timmermann, R., Hellmer, H. H., et al. (2018). Intercomparison of Antarctic ice-shelf, ocean, and sea-ice interactions simulated by MetROMS-iceshelf and FESOM 1.4. *Geoscientific Model Development*, *11*(4), 1257–1292. https://doi.org/10.5194/gmd-11-1257-2018

Rignot, E., Jacobs, S., Mouginot, J., & Scheuchl, B. (2013). Ice-shelf melting around Antarctica. *Science*, *341*(6143), 266–270. https://doi.org/10.1126/science.1235798

Sallée, J. B., Shuckburgh, E., Bruneau, N., Meijers, A. J., Bracegirdle, T. J., Wang, Z., & Roy, T. (2013). Assessment of Southern Ocean water mass circulation and characteristics in CMIP5 models: Historical bias and forcing response. *Journal of Geophysical Research: Oceans*, *118*(4), 1830–1844. https://doi.org/10.1002/jgrc.20135

Shean, D. E., Joughin, I. R., Dutrieux, P., Smith, B. E., & Berthier, E. (2019). Ice shelf basal melt rates from a high-resolution digital elevation model (DEM) record for Pine Island Glacier, Antarctica. *The Cryosphere*, *13*(10), 2633–2656. https://doi.org/10.5194/tc-13-2633-2019

Wang, Z. (2013). On the response of Southern Hemisphere subpolar gyres to climate change in coupled climate models. *Journal of Geophysical Research: Oceans*, *118*(3), 1070–1086. https://doi.org/10.1002/jgrc.20111